International Journal of Bridge Engineering (IJBE), Vol. 3, No. 2, (2015), pp. 49-76

THE INFLUENCE OF CURVATURE AND OTHER PARAMETERS ON THE DYNAMIC BEHAVIOR OF CURVED BRIDGES

Tassos P. Avraam[1], George T. Michaltsos[2]

Department of Civil Engineering, National Technical University of Athens
9 Iroon Polytechneiou Str., Zografou Campus, Athens15780, Greece
e-mail: avraamt@central.ntua.gr, michalts@central.ntua.gr

ABSTRACT: The present study deals with the behavior of curved-in-plane bridges and examines the effect of the radius of curvature, the vehicle speed, the section slope (superelevation), the pavement situation and mainly the achievable accuracy depending on the vehicle model used. In this paper, besides the above parameters, the influence of loading model is studied, especially the models of a concentrated load, a sequence of two concentrated loads and finally a real vehicle where its width is taken into account where the loads are considered as concentrated ones. A 3-DOF model is considered to study the bridge, while the theoretical formulation is based on a continuum approach, which has been widely used in the literature to analyze such bridges.

KEY WORDS: Bridges' Dynamics; Curved Bridges; Moving loads.

1. INTRODUCTION

A lot of work has been reported during the last 100 years dealing with the dynamic response of railway bridges and later of highway bridges, under the influence of moving loads. Extensive references to the literature on this subject can be found in the excellent Frýba's book [1].
Two early contributions, in this area, presented by Stokes [2] and Zimmerman [3] are very interesting. In 1905, Krýlov [4] gave a complete solution to the problem of the dynamic behavior of a prismatic bar acted upon by a load of constant magnitude, moving with a constant velocity. In 1922, Timoshenko [5] solved the same problem but for a harmonic pulsating moving force. Another pioneer work on this subject was presented in 1934 by Inglis [6], in which several parameters were taken into account. In 1951, Hillerborg [7] gave an analytical solution to the previous problem by means of Fourier's method.
Despite the availability of high speed computers most of the methods used today for analyzing bridge vibration problems are essentially based on the Inglis's or Hillerborg's early techniques. Relevant publications are the ones of

Steuding [8] ,Honda et al [9], Gillespi [10], Green and Cebon [11], Lee [12], Michaltsos et al [13], Xu and Genin [14] , Foda and Abduljabbar [15], Michaltsos [16] and [17].

On the other hand, in practice, in spite of the great number of works for over 50 years, bridges (as also other constructions which are acted upon by dynamic loads) have been designed accounting dynamic loads by increasing the design live loads by a semi-empirical "impact factor" or "dynamic load factor".

Recently, there have been many programs of research, discussing the effect of the characteristics of a bridge or a vehicle on the dynamic response of a bridge such as: the programs in U.S.A [18], in U.K. and Canada [19], in the Organization for Economic Cooperation and Development (O.E.C.D.) [20], in Switzerland [21] etc.

Among the important studies in this field, we must especially refer to the important experimental research by Cantieri [22] dealing with different models of moving loads.

Curved reinforced concrete or steel bridges are very common as elements of highway access, ramps and interchanges, while they are often the only solution in special territories.

A wide field of research is that of seismic behavior of curved bridges.

A majority of experimental and numerical research on horizontally curved bridges was done in the U.S. in the late 1960s and early 1970s e.g. Mozer and Culver [23], Culver [24], Brennan [25]. This research continued in the 1990s (Yoo and Carbine [26]; Zureick et al. [27]) and was used to improve the American Association of State Highway and Transportation Officials (AASHTO) specifications concerning this topic. The aforementioned research was mainly related to steel bridges.

The seismic behaviour of bridges is principally influenced by the seismic response of the substructures: bridge columns, abutments and foundations. In fact, design codes such as the Caltrans Seismic Design Criteria in California (Caltrans [29]) and the Eurocodes in Europe (CEN) [28] assume that the bridge deck remains elastic during a seismic event, and that the energy introduced by the ground motion is dissipated by either the substructures or specific seismic isolation and/or damping devices.

Parametric analyses related to the seismic behavior of curved bridges have recently been carried out by Abdel-Salam and Heins [30], Wu and Najjar [31] and Linzell and Nadakuditi [32]. This last paper highlighted that the radius of curvature had the greatest influence on the seismic response of curved steel I-girder simply supported bridges. These papers address horizontally curved steel bridges.

The present paper deals with the behaviour of curved-in-plane bridges and examines the effect of the radius of curvature, the vehicle speed, the section slope(superelevation), the pavement situation and mainly the achievable accuracy depending on the vehicle model used.

In this precursor study besides the above parameters, the influence of loading model is studied, especially the models of a concentrated load, a sequence of two concentrated loads and finally a real vehicle where its width is taken into account where the loads are considered as concentrated ones. In a later paper, the models of damped-mass-loads and of damped-vehicle will be studied.
A 3-DOF model is considered to study the bridge model, while the theoretical formulation is based on a continuum approach, which has been widely used in the literature to analyze such bridges.

2. MATHEMATICAL FORMULATION

2.1. The equations of motion

Let us consider now the deck of the bridge that is shown in Fig. 1 by the gravity centers' line of its cross-sections (OS).
The length L of the a curved-in-plane bridge with radius of curvature R, is given by the relation $L = R \cdot \rho$, where ρ is the sectorial angle that corresponds to the length L.
A random point A of the bridge can be determined by the angle ϑ.
We assume that the distance z_M between the shear center M and the gravity center S is very small compared to the radius R.
The above assumption means that we accept that the torsional moment m_x acts about the axis of gravity centers (while in reality it acts about the axis of the shear centers).

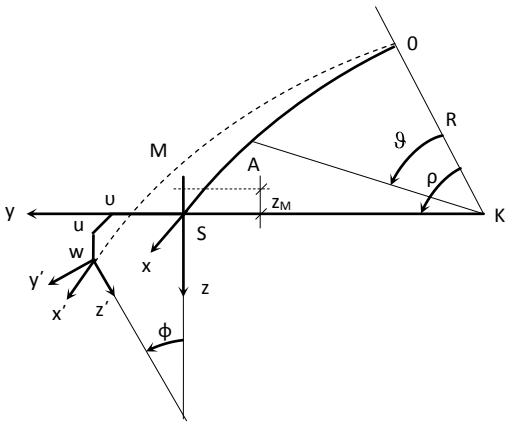

Fig. 1: The deck's displacements

According to the theory of curved beams with thin-walled cross-sections, the following equations are valid [33]:

$$\left.\begin{aligned}
&E J_z v'''' + \frac{2 E J_z}{R^2}\cdot v'' + \frac{E J_z}{R^4}\cdot v + c_y \dot{v} + m\ddot{v} = q_y \\
&\left(E J_y - \frac{E J_\omega}{R^2}\right) w'''' + \frac{G J_d}{R^2}\cdot w'' - \frac{E J_y - G J_d}{R}\cdot \varphi'' - \frac{E J_\omega}{R}\cdot \varphi'''' + c_z \dot{w} + m\ddot{w} = q_z \\
&E J_\omega \varphi'''' - G J_d \varphi'' - \frac{E J_y}{R^2}\cdot \varphi + \frac{E J_\omega}{R}\cdot w'''' + \frac{E J_y - G J_d}{R}\cdot w'' + c_\varphi \dot{\varphi} + J_{px}\ddot{\varphi} = m_x
\end{aligned}\right\} \quad (1)$$

where q_y, q_z and m_x are the internal forces developed on the cross-section at $x = R\cdot\vartheta$ (see fig. 1), while J_{px} is the torsional mass-moment of inertia about the x-axis. In the present analysis, we will proceed for the usual case where m_y=m_z=0 (for the directions and axes x, y, z, see figure 1).
For the following analysis and in order to apply the Galerkin's procedure, we need a suitable set of expressions for the v, w, φ.

2.2. Set of expressions v, w, φ

Considering the case of a free vibrating bridge and ignoring, for instant, the effect of the torsion on the vertical bending, equations (1) become:

$$\left.\begin{aligned}
&E J_z v'''' + \frac{2 E J_z}{R^2}\cdot v'' + \frac{E J_z}{R^4}\cdot v + c_y \dot{v} + m\ddot{v} = 0 \\
&\left(E J_y - \frac{E J_\omega}{R^2}\right) w'''' + \frac{G J_d}{R^2}\cdot w'' + c_z \dot{w} + m\ddot{w} = 0 \\
&E J_\omega \varphi'''' - G J_d \varphi'' - \frac{E J_y}{R^2}\cdot \varphi + \frac{E J_\omega}{R}\cdot w'''' + \frac{E J_y - G J_d}{R}\cdot w'' + c_\varphi \dot{\varphi} + J_{px}\ddot{\varphi} = 0
\end{aligned}\right\} \quad (2a,b,c)$$

Equation (2a) shows that the lateral motion is independent of the others, while vertical and torsional ones are coupled. Thus we put:

$$\left.\begin{aligned}
v(x,t) &= Y(x)\cdot T_y(t) \\
w(x,t) &= Z(x)\cdot T_z(t) \\
\varphi(x,t) &= \Phi(x)\cdot T_z(t)
\end{aligned}\right\} \quad (2d,e,f)$$

2.2.1 The lateral motion

Introducing (2d) into (2a), we conclude to the following uncoupled equations:

$$\left.\begin{aligned}
&E I_z Y''''(x) + \frac{2 E I_z}{R^2} Y''(x) + \frac{E I_z}{R^4} Y(x) - m\omega_y^2 Y(x) = 0 \\
&\ddot{T}_y + \frac{c_y}{m}\dot{T}_y + \omega_y^2 T_y = 0
\end{aligned}\right\} \quad (3a,b)$$

The solution of (3a) gives the eigenshapes of lateral motion:

$$\left.\begin{aligned} &Y_n(x)=c_1\left(\sin\lambda_{1n}x+\frac{\sin\lambda_{1n}L}{\operatorname{Sinh}\lambda_{2n}L}\cdot\operatorname{Sinh}\lambda_{2n}x\right)\\ &\text{where:}\quad \lambda_{1n}=\sqrt{\frac{1}{R^2}+\sqrt{\frac{m\,\omega_{yn}^2}{E\,J_z}}}\quad,\quad \lambda_{2n}=\sqrt{-\frac{1}{R^2}+\sqrt{\frac{m\,\omega_{yn}^2}{E\,J_z}}}\\ &\text{and:}\qquad \omega_{yn}^2=\frac{E\,J_z}{m}\cdot\left(\frac{n^2\pi^2}{L^2}-\frac{1}{R^2}\right)^2 \end{aligned}\right\}\qquad (3c,d,e,f)$$

2.2.2. The vertical-torsional motion

Introducing (2e,f) into (2b,c) we obtain the following equations:

$$\left.\begin{aligned} &\left(E\,J_y-\frac{E\,J_\omega}{R^2}\right)Z''''+\frac{G\,J_d}{R^2}\cdot Z''-m\,\omega_z^2\,Z=0\\ &E\,J_\omega\Phi''''-G\,J_d\,\Phi''-\frac{E\,J_y}{R^2}\cdot\Phi+\frac{E\,J_\omega}{R}\cdot Z''''+\frac{E\,J_y-G\,J_d}{R}\cdot Z''-J_{px}\omega_z^2\,\Phi=0\\ &\ddot{T}_z+\frac{c_z}{m}\dot{T}+\omega_z^2\,T_z=0 \end{aligned}\right\}\qquad (4a,b,c)$$

The first of equations (4) gives:

$$\left.\begin{aligned} &Z_n(x)=c_1\left(\sin k_{1n}x+\frac{\sin k_{1n}L}{\operatorname{Sinh}k_{2n}L}\cdot\operatorname{Sinh}k_{2n}x\right)\\ &\text{where:}\\ &k_{1n}=\sqrt{\frac{G\,J_d}{2(R^2E\,J_y-EJ_\omega)}+\sqrt{\left(\frac{G\,J_d}{2(R^2E\,J_y-EJ_\omega)}\right)^2+\frac{R^2m\,\omega_{zn}^2}{R^2E\,J_y-EJ_\omega}}}\\ &k_{2n}=\sqrt{-\frac{G\,J_d}{2(R^2E\,J_y-EJ_\omega)}+\sqrt{\left(\frac{G\,J_d}{2(R^2E\,J_y-EJ_\omega)}\right)^2+\frac{R^2m\,\omega_{zn}^2}{R^2E\,J_y-EJ_\omega}}}\\ &\text{and:}\quad \omega_{zn}^2=\frac{R^2E\,J_y-EJ_\omega}{R^2m}\cdot\frac{n^2\pi^2}{L^2}\cdot\left(\frac{n^2\pi^2}{L^2}+\frac{G\,J_d}{R^2E\,J_y-EJ_\omega}\right) \end{aligned}\right\}\qquad (4,d,e,f,g)$$

The second of eqs (4) becomes:

$$EJ_\omega\Phi_n''''-GJ_d\Phi_n''-\frac{EJ_y}{R^2}\Phi_n-\omega_{zn}^2J_{px}\Phi_n=-\frac{EJ_y}{R}Z_n''''-\frac{EJ_y-GJ_d}{R}Z_n''$$

The above due to the first of eq.(4) becomes:

$$\left.\begin{aligned} &EJ_\omega \Phi_n''' - GJ_d \Phi_n'' - \frac{EJ_y}{R^2}\Phi_n - \omega_{zn}^2 J_{px}\Phi_n = \zeta_{1n}\sin k_{1n}x + \zeta_{2n}\sinh k_{2n}x \\ &\text{where:}\quad \zeta_{1n} = k_{1n}^2\left(-k_{1n}^2\frac{EJ_\omega}{R} + \frac{EJ_y - GJ_d}{R}\right) \\ &\qquad\quad \zeta_{2n} = -k_{2n}^2\left(k_{2n}^2\frac{EJ_\omega}{R} + \frac{EJ_y - GJ_d}{R}\right)\frac{\sin k_{1n}L}{\sinh k_{2n}L} \end{aligned}\right\} \qquad (5a,b,c))$$

The solution of the above (5a) is:

$$\Phi_n(x) = c_1\sin\mu_{1n}x + c_2\cos\mu_{1n}x + c_3\sinh\mu_{2n}x + c_4\cosh\mu_{2n}x + A_n\sin k_{1n}x + B_n\cos k_{2n}x \qquad (5d)$$

Where:

$$\left.\begin{aligned} A_n &= \frac{\zeta_{1n}}{EJ_\omega k_{1n}^4 + GJ_d k_{1n}^2 - EJ_\omega/R^2 - \omega_{zn}^2 J_{px}} \\ B_n &= \frac{\zeta_{2n}}{EJ_\omega k_{1n}^4 - GJ_d k_{1n}^2 - EJ_\omega/R^2 - \omega_{zn}^2 J_{px}} \\ \mu_{1n} &= \sqrt{-\frac{GJ_d}{2EJ_\omega} + \sqrt{\left(\frac{GJ_d}{2EJ_\omega}\right)^2 + \frac{J_{px}\omega_{\varphi n}^2}{EJ_\omega} + \frac{J_y}{R^2 J_\omega}}} \\ \mu_{2n} &= \sqrt{\frac{GJ_d}{2EJ_\omega} + \sqrt{\left(\frac{GJ_d}{2EJ_\omega}\right)^2 + \frac{J_{px}\omega_{\varphi n}^2}{EJ_\omega} + \frac{J_y}{R^2 J_\omega}}} \end{aligned}\right\} \qquad (5e,f,g,h)$$

The boundary conditions are: $\Phi(0) = \Phi(L) = \Phi''(0) = \Phi''(L) = 0$, from which one can determine:

$$\left.\begin{aligned} c_{2n} &= 0 \\ c_{4n} &= 0 \\ c_{1n} &= \frac{-A_n(k_{1n}^2 + \mu_{1n}^2)\sin k_{1n}L + B_n(k_{2n}^2 - \mu_{2n}^2)\sinh k_{2n}L}{(\mu_{1n}^2 + \mu_{2n}^2)\sin\mu_{1n}L} \\ c_{3n} &= \frac{A_n(k_{1n}^2 - \mu_{1n}^2)\sin k_{1n}L - B_n(k_{2n}^2 + \mu_{2n}^2)\sinh k_{2n}L}{(\mu_{1n}^2 + \mu_{2n}^2)\sinh\mu_{2n}L} \end{aligned}\right\} \qquad (6a,b,c,d)$$

and finally:

$$\Phi_n(x) = c_{1n}\sin\mu_{1n}x + c_{3n}\sinh\mu_{2n}x + A_n\sin k_{1n}x + B_n\cos k_{2n}x \qquad (6e)$$

3. THE FREE VIBRATING BRIDGE

The equations for the free motion of the bridge are:

$$\left.\begin{aligned} &EJ_z v'''' + \frac{2EJ_z}{R^2}\cdot v'' + \frac{EJ_z}{R^4}\cdot v + m\ddot{v} = 0 \\ &\left(EJ_y - \frac{EJ_\omega}{R^2}\right)w'''' + \frac{GJ_d}{R^2}\cdot w'' - \frac{EJ_y - GJ_d}{R}\cdot\varphi'' - \frac{EJ_\omega}{R}\cdot\varphi'''' + m\ddot{w} = 0 \\ &EJ_\omega\varphi'''' - GJ_d\varphi'' - \frac{EJ_y}{R^2}\cdot\varphi + \frac{EJ_\omega}{R}\cdot w'''' + \frac{EJ_y - GJ_d}{R}\cdot w'' + J_{px}\ddot{\varphi} = 0 \end{aligned}\right\} \quad (7a,b,c)$$

3.1. The horizontal motion

The first of equations (7), is independent of the two others.
Therefore its eigenfrequencies and shape functions are given by equations (3c,d,e,f).

3.2. The couplet vertical-torsional motion

In order to elaborate equations (7b,c), we are searching for a solution of the form:

$$\left.\begin{aligned} w(x,t) &= W(x)\cdot T(t) \\ \varphi(x,t) &= \Theta(x)\cdot T(t) \end{aligned}\right\} \quad (8a,b)$$

Introducing eqns (8) into eqns (7b,c), we arrive to the following differential system:

$$\left.\begin{aligned} &S_1\cdot W'''' + \frac{GJ_d}{R^2}\cdot W'' - S_2\cdot\Theta'' - \frac{EJ_\omega}{R}\cdot\Theta'''' - m\omega^2 W = 0 \\ &EJ_\omega\Theta'''' - GJ_d\Theta'' - \frac{EJ_y}{R^2}\cdot\Theta + \frac{EJ_\omega}{R}\cdot W'''' + S_2\cdot W'' - J_{px}\omega^2\Theta = 0 \\ &\text{where:}\quad S_1 = EJ_z - \frac{EJ_\omega}{R^2},\quad S_2 = \frac{EJ_z - GJ_d}{R} \end{aligned}\right\} \quad (9a,b,c,d)$$

In order to apply the Galerkin procedure we set:

$$\left.\begin{aligned} W_\rho(x) &= a_{\rho1}Z_1(x) + a_{\rho2}Z_2(x) + \cdots + a_{\rho n}Z_n(x) \\ \Theta_\rho(x) &= b_{\rho1}\Phi_1(x) + b_{\rho2}\Phi_2(x) + \cdots + b_{\rho n}\Phi_n(x) \end{aligned}\right\} \quad (10a,b)$$

where a_i and b_i are unknown coefficients to be determined and Z_i, Φ_i, are arbitrarily chosen functions of x, which satisfy the boundary conditions. As such functions we choose the expressions given by eqns (4a) and (6e). Functions W_k and Θ_k, corresponding to the eigenfrequency ω_k will be determined below.
Introducing eqns (10) into eqns (9), multiplying the out come successively the first by Z_1, Z_2, ….,Z_n and the second by Φ_1, Φ_2, …, Φ_n, and integrating from 0 to L, we obtain the following linear homogeneous system with unknown the coefficients $a_{\rho i}$ and $b_{\rho i}$.

$$\left.\begin{aligned}
&\sum_{i=1}^{n} a_{\rho i}\left(S_1 \int_0^L Z_i'''' Z_\sigma dx + \frac{G J_d}{R^2} \int_0^L Z_i'' Z_\sigma dx + m\omega^2 \int_0^L Z_i Z_\sigma dx \right) - \\
&\qquad \sum_{i=1}^{n} b_{\rho i}\left(S_2 \int_0^L \Phi_i'' Z_\sigma + \frac{E J_\omega}{R} \int_0^L \Phi_i'''' Z_\sigma dx \right) = 0 \\
&\sum_{i=1}^{n} a_{\rho i}\left(\frac{E J_\omega}{R} \int_0^L Z_i'''' \Phi_\sigma dx + S_2 \int_0^L Z_i'' \Phi_\sigma dx \right) + \\
&\sum_{i=1}^{n} b_{\rho i}\left(E J_\omega \int_0^L \Phi_i'''' \Phi_\sigma dx - G J_d \int_0^L \Phi_i'' \Phi_\sigma dx - \left(\frac{E J_y}{R^2} + \omega^2 J_{px} \right) \int_0^L \Phi_i \Phi_\sigma dx \right) = 0
\end{aligned}\right\} \qquad (11)$$

with $\sigma = 1 \text{ to } n$ and $\rho = 1 \text{ to } n$.

Equations (11) represent a linear system of homogeneous equations with unknowns $a_{\rho i}$ and $b_{\rho i}$. For a non trivial solution of equations (11), the determinant of the coefficients of the unknowns must be equal to zero, i.e.:

$$\left| \Delta_{ij} \right| = 0 \qquad (12)$$

from which the eigenfrequencies of the bridge can be determined.

Neglecting the first line of equations (11) and solving the remaining equations, we can determine the constants a_i $(i = 2 \text{ to } n)$ and b_i $(i = 1 \text{ to } n)$, with respect to a_i and thus the eigenfunctions to vertical-torsional motion of the bridge.

3.3. The orthogonality conditions

Easily, through the known process, one can determine the following orthogonality conditions for the eigenshapes determined according to the previous paragraphs 3.1 and 3.2:

3.3.1 For the lateral motion

$$\int_0^L Y_n Y_k dx = \begin{cases} 0 & \text{for} \quad n \neq k \\ \Gamma_k & \text{for} \quad n = k \end{cases} \qquad (13)$$

3.3.2 For the vertical-torsional motion

$$\int_0^L (m W_n W_k + J_{px} \Theta_n \Theta_k) dx = \begin{cases} 0 & \text{for} \quad n \neq k \\ \Gamma_k & \text{for} \quad n = k \end{cases} \qquad (14)$$

4. THE FORCED VIBRATING BRIDGE

4.1. The horizontal motion

The equation of motion is:

$$E J_z v'''' + \frac{2 E J_z}{R^2} \cdot v'' + \frac{E J_z}{R^4} \cdot v + c_y \dot{v} + m \ddot{v} = q_y(x,t) = \bar{q}_y(x) \cdot f(t) \tag{15}$$

We are searching for a solution of the form:

$$v = \sum_n Y_n(x) \cdot T_n(t) \tag{16a}$$

where $Y_n(x)$ are the eigenforms of the bridge given by equ (3a) and $T_n(t)$ the time functions to be determined. Introducing (16a) into (15) we get:

$$E J_z \sum_n Y_n'''' T_n + \frac{2 E J_z}{R^2} \sum_n Y_n'' T_n + \frac{E J_z}{R^4} \sum_n Y_n T_n + c_y \sum_n Y_n \dot{T}_n + m \sum_n Y_n \ddot{T}_n = \bar{q}_y f(t)$$

Remembering that $Y_n(x)$ satisfies the equation of free motion (3a), the above becomes:

$$m \sum_n Y_n \ddot{T}_n + c_y \sum_n Y_n \dot{T}_n + m \sum_n \omega_{yn}^2 Y_n T_n = \bar{q}_y(x) f(t) \tag{16b}$$

Multiplying the above by Y_ρ and taking into account the orthogonality condition we conclude to the following equation:

$$\ddot{T}_\rho(t) + \frac{c_y}{m} \dot{T}_\rho(t) + \omega_{y\rho}^2 T_\rho(t) = \frac{1}{m \int_0^L Y_\rho^2 dx} \cdot \int_0^L \bar{q}_y(x) Y_\rho(x) dx \cdot f(t) \tag{16c}$$

The solution of the above is given by the Duhamel's integral:

$$\left.\begin{aligned} T_\rho(t) &= \frac{\int_0^L \bar{q}_y(x) Y_\rho(x) dx}{m \bar{\omega}_{y\rho} \int_0^L Y_\rho^2 dx} \cdot \int_0^t e^{-\beta(t-\tau)} f(\tau) \cdot \sin \bar{\omega}_{y\rho}(t-\tau)\, d\tau \\ \text{with}: \quad \beta &= \frac{c_y}{2m}, \quad \bar{\omega}_{y\rho}^2 = \omega_{y\rho}^2 - \beta^2 \end{aligned}\right\} \tag{16d}$$

4.2. The lateral-torsional motion

The equations of motion are:

$$\left.\begin{aligned} &\left(E J_y - \frac{E J_\omega}{R^2}\right) w'''' + \frac{G J_d}{R^2} \cdot w'' - \frac{E J_y - G J_d}{R} \cdot \varphi'' - \frac{E J_\omega}{R} \cdot \varphi'''' + c_z \dot{w} + m \ddot{w} = \bar{q}_z(x) f_z(t) \\ &E J_\omega \varphi'''' - G J_d \varphi'' - \frac{E J_y}{R^2} \cdot \varphi + \frac{E J_\omega}{R} \cdot w'''' + \frac{E J_y - G J_d}{R} \cdot w'' + c_\varphi \dot{\varphi} + J_{px} \ddot{\varphi} = \bar{m}_x(x) f_\varphi(t) \end{aligned}\right\} \tag{17a,b}$$

We are searching for a solution of the form:

$$\left.\begin{aligned} w(x,t) &= \sum_n W_n(x)\cdot P_n(t) \\ \varphi(x,t) &= \sum_n \Theta_n(x)\cdot P_n(t) \end{aligned}\right\} \qquad (18a,b)$$

where W_n and Θ_n are the eigenshapes of the bridge given by eqns (10a,b) and $P_n(t)$ the time functions to be determined. Introducing (18a,b) into (17a,b) we get:

$$\left.\begin{aligned} &S_1\sum_n W_n'''' P_n + \frac{GJ_d}{R^2}\sum_n W_n'' P_n - S_2\sum_n \Theta_n'' P_n - \frac{EJ_\omega}{R}\sum_n \Theta_n'''' P_n + c_z\sum_n W_n\dot{P}_n + m\sum_n W_n\ddot{P}_n = \\ &\qquad = \bar{q}_z(x)\cdot f_z(t) \\ &EJ_\omega\sum_n \Theta_n'''' P_n - GJ_d\sum_n \Theta_n'' P_n - \frac{EJ_y}{R^2}\sum_n \Theta_n P_n + \frac{EJ_\omega}{R}\sum_n W_n'''' P_n + S_2\sum_n W_n'' P_n + c_\varphi\sum_n \Theta_n\dot{P}_n + \\ &\qquad + J_{px}\sum_n \Theta_n\ddot{P}_n = \bar{m}_x(x)\cdot f_\varphi(t) \end{aligned}\right\} \qquad (18c,d)$$

Remembering that W_n and Θ_n satisfy the equations of the free motion (9a,b), the above become:

$$\left.\begin{aligned} &m\sum_n W_n\ddot{P}_n + c_z\sum_n W_n\dot{P}_n + m\sum_n \omega_{zn}^2 W_n P_n = \bar{q}_z(x)\cdot f_z(t) \\ &J_{px}\sum_n \Theta_n\ddot{P}_n + c_\varphi\sum_n \Theta_n\dot{P}_n + J_{px}\sum_n \omega_{zn}^2\Theta_n P_n = \bar{m}_x(x)\cdot f_\varphi(t) \end{aligned}\right\} \qquad (19a,b)$$

Multiplying (19a) by W_ρ and integrating from 0 to L, the (19b) by Θ_ρ and integrating from 0 to L, and remembering that $c_\varphi = c_z J_{px}/m$, the above become:

$$\left.\begin{aligned} &\sum_n \int_0^L mW_nW_\rho dx\cdot(\ddot{P}_n + \frac{c_z}{m}\dot{P}_n + \omega_{zn}^2 P_n) = f_z(t)\int_0^L \bar{q}_z\cdot W_\rho dx \\ &\sum_n \int_0^L J_{px}\Theta_n\Theta_\rho dx\cdot(\ddot{P}_n + \frac{c_z}{m}\dot{P}_n + \omega_{zn}^2 P_n) = f_\varphi(t)\int_0^L \bar{m}_x\cdot\Theta_\rho dx \end{aligned}\right\} \qquad (20a,b)$$

Adding the above equations and taking into account the orthogonality condition we get:

$$\ddot{P}_\rho + \frac{c_z}{m}\dot{P} + \omega_{z\rho}^2 = \frac{1}{m\int_0^L W_\rho^2 dx + J_{px}\int_0^L \Theta_\rho^2 dx}\left(f_z(t)\int_0^L \bar{q}_z W_\rho dx + f_\varphi(t)\int_0^L \bar{m}_x\Theta_\rho dx\right) \qquad (20c)$$

The solution of the above (20c) is given by the Duhamel's integral:

$$P_\rho(t)=\left.\begin{aligned}&\frac{\int_0^L \bar{q}_z W_\rho dx}{\bar{\omega}_{z\rho}\left(m\int_0^L W_\rho^2 dx + J_{px}\int_0^L \Theta_\rho^2 dx\right)}\cdot\int_0^t e^{-\beta(t-\tau)}\cdot f_z(\tau)\cdot \sin\bar{\omega}_{z\rho}(t-\tau)d\tau + \\ &+\frac{\int_0^L \bar{m}_x \Theta_\rho dx}{\bar{\omega}_{z\rho}\left(m\int_0^L W_\rho^2 dx + J_{px}\int_0^L \Theta_\rho^2 dx\right)}\cdot\int_0^t e^{-\beta(t-\tau)}\cdot f_\varphi(\tau)\cdot \sin\bar{\omega}_{z\rho}(t-\tau)d\tau\end{aligned}\right\} \quad (21)$$

where $\beta=\frac{c_z}{2m}$, $\bar{\omega}_{z\rho}^2=\omega_{z\rho}^2-\beta^2$.

5. THE MOVING LOADS

In this section we will study firstly the behavior of a curved-in-plane bridge under the action of a concentrated load, moving with speed υ, and after of a vehicle moving with speed υ.

In figure 2, the bridge and its cross-section for the above loading case are shown.

Usually, a section slope φ (fig.2) exists on the curved parts of road bridges. Although slope φ, is important and necessary in railway bridges, it has not the same significant influence on road bridges, because it is always smaller than 5^o (while in railway bridges it can be up to 10^o).

Let us see the influence of the angle φ on the allowed safe speed υ of the moving load.

Symbolizing with μ the friction coefficient, the equilibrium of the horizontal forces gives: $\frac{M\cdot\upsilon^2}{R}=\mu Mg+MgSin\varphi$, which concludes to the following inequality for the allowed speed υ:

$$\upsilon\le\sqrt{R\cdot g\cdot(\mu+Sin\varphi)} \quad (22)$$

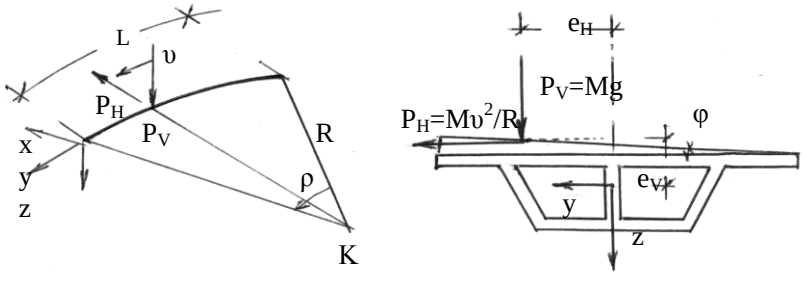

Fig. 2: The moving Load

The values of the coefficient of friction μ between car tires and asphalt, given by the relative manuals are:

$$\left.\begin{array}{l}\mu = 0.72 \quad \text{for dry surfaces} \\ \mu = 0.35 \quad \text{for wet surfaces}\end{array}\right\}$$

In the plots of figure 3 one can see the influence of angle φ on the load speed υ for both dry and wet deck surface for three characteristic radius of curvature R=50m (fig.3a), R=100m (fig.3b) and R=150m (fig.3c)

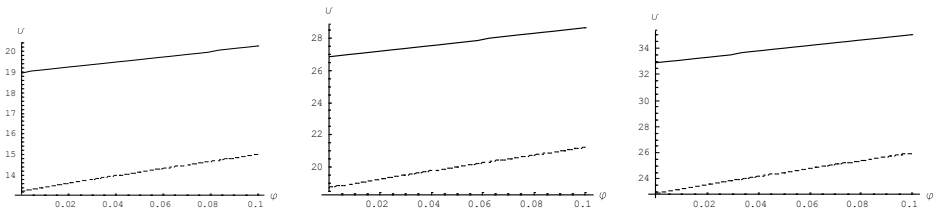

(3a) (3b) (3c)

Fig. 3: The influence of section slope φ on the allowed speed υ.
(__) dry deck surface, (…..) wet deck surface

\

In table 1 the allowed speeds in m/sec, and the achieved increase of the allowed speeds (in percentage) for $\varphi = 5^o$ and for both, dry and wet deck surface and the above chosen radius are shown.

TABLE 1

	R=50 m			**R=100 m**			**R=150 m**		
φ	**5^o**	**0^o**	**%**	**5^o**	**0^o**	**%**	**5^o**	**0^o**	**%**
Dry	**20.25**	**18.80**	**7.7**	**28.80**	**26.80**	**7.4**	**35.10**	**32.90**	**6.6**
wet	**15.10**	**13.20**	**14.4**	**21.30**	**18.65**	**14.3**	**26.10**	**22.90**	**13.9**

5.1. The concentrated moving load

In this case the right side members of equation (4) become:

$$\left.\begin{array}{l} q_y = \dfrac{M \cdot \upsilon^2}{R + e_H} \cdot \delta(x - \alpha) \\ q_z = M \cdot g \cdot \delta(x - \alpha) \\ m_x = \left(M \cdot g \cdot e_H + \dfrac{M \cdot \upsilon^2}{R + e_H} \cdot e_V \right) \cdot \delta(x - \alpha) \end{array}\right\} \qquad (23a,b,c)$$

where δ is the Dirac delta function and α is the position of the load P at time t.

5.1.1. The lateral motion

Introducing (23a) into the right side member of equation (15), and following the process of paragraph 4.1, we conclude to the following equation:

$$\ddot{T}_\rho + \frac{c_y}{m}\dot{T}_\rho + \omega_{y\rho}^2 T_\rho = \frac{1}{m\int_0^L Y_\rho^2 dx}\int_0^t \frac{M\upsilon^2}{R+e_H} Y_\rho(x)\delta(x-\alpha)dx = \frac{M\upsilon^2}{m(R+e_H)\int_0^L Y_\rho^2 dx} Y_\rho(\alpha)$$

Or finally:

$$\ddot{T}_\rho + \frac{c_y}{m}\dot{T}_\rho + \omega_{y\rho}^2 T_\rho = \frac{M\upsilon^2}{m(R+e_H)\int_0^L Y_\rho^2 dx} Y_\rho(\upsilon t)\,,$$

which has the solution:

$$T_\rho = \frac{M\upsilon^2}{m(R+e_H)\overline{\omega}_{y\rho}\int_0^L Y_\rho^2 dx}\int_0^t e^{-\beta(t-\tau)} Y_\rho(\upsilon\tau)\,\mathrm{Sin}\,\overline{\omega}_{y\rho}(t-\tau)\,d\tau \qquad (24)$$

with β and $\overline{\omega}_{y\rho}$ from equation (16).

5.1.2. The vertical-torsional motion

Introducing (23b,c) into the right side members of eqns (20a,b) and following the process of paragraph 4.2, we conclude to the following equation:

$$\ddot{P}_\rho + \frac{c_z}{m}\dot{P}_\rho + \omega_{z\rho}^2 P_\rho = \frac{M\cdot g\cdot Z_\rho(\upsilon t) + \left(M\cdot g\cdot e_H + \frac{M\upsilon^2}{R+e_H}e_V\right)\Theta_\rho(\upsilon t)}{m\int_0^L Z_\rho^2 dx + J_{px}\int_0^L \Theta_\rho^2 dx}\,,$$

which has the solution:

$$\left.\begin{aligned} P_\rho = {} & \frac{M\cdot g\cdot Z_\rho(\upsilon t)}{\left(m\int_0^L Z_\rho^2 dx + J_{px}\int_0^L \Theta_\rho^2 dx\right)}\int_0^L e^{-\beta(t-\tau)}\cdot Z_\rho(\upsilon\tau)\cdot \mathrm{Sin}\,\overline{\omega}_{z\rho}(t-\tau)\,d\tau + \\ & + \frac{M\cdot g\cdot e_H + \frac{M\upsilon^2}{R+e_H}e_V}{\left(m\int_0^L Z_\rho^2 dx + J_{px}\int_0^L \Theta_\rho^2 dx\right)}\int_0^L e^{-\beta(t-\tau)}\cdot \Theta_\rho(\upsilon\tau)\cdot \mathrm{Sin}\,\overline{\omega}_{z\rho}(t-\tau)\,d\tau \end{aligned}\right\} \qquad (25)$$

5.2. The moving vehicle

Considering the vehicle of figure 4, this case of loading can be easily solved following the known procedure with external loads:

$$\left.\begin{aligned}
q_y &= \left(\frac{M\cdot\upsilon^2}{4(R+e_H-b)}+\frac{M\cdot\upsilon^2}{4(R+e_H+b)}\right)\cdot\delta(x-\alpha)\\
&\quad+\left(\frac{M\cdot\upsilon^2}{4(R+e_H-b)}+\frac{M\cdot\upsilon^2}{4(R+e_H+b)}\right)\cdot\delta(x-\alpha+2d)\\
q_z &= \frac{M\cdot g}{2}\cdot\delta(x-\alpha)+\frac{M\cdot g}{2}\cdot\delta(x-\alpha+2d)\\
m_x &= \left(\frac{M\cdot g}{4}+\frac{F_c e_V}{4b}\right)(e_H+b)\cdot\delta(x-\alpha)+\left(\frac{M\cdot g}{4}-\frac{F_c e_V}{4b}\right)(e_H-b)\cdot\delta(x-\alpha)\\
&\quad+\left(\frac{M\cdot g}{4}+\frac{F_c e_V}{4b}\right)(e_H+b)\cdot\delta(x-\alpha+2d)+\left(\frac{M\cdot g}{4}-\frac{F_c e_V}{4b}\right)(e_H-b)\cdot\delta(x-\alpha+2d)
\end{aligned}\right\} \quad (26a,b,c)$$

The first members of (26a), (26b), and the first two of (26c) are valid for $0\le t\le L/\upsilon$, while the second members of (26a), (26b), and the third and fourth members of (26c) are valid for $2d/\upsilon\le t\le (L+2d)/\upsilon$.

5.2.1. The lateral motion

Introducing (26a) into the right side member of equ (15), and following the process of §4.1 we conclude to the following equation:

$$T_\rho = \frac{Q_y}{m\bar{\omega}_{y\rho}\int_0^L Y_\rho^2 dx}\left\{\left(\int_0^t e^{-\beta(t-\tau)}Y_\rho(\upsilon\tau)\,\mathrm{Sin}\,\bar{\omega}_{y\rho}(t-\tau)\,d\tau\right)\cdot\left[1-H\left(1-\frac{L}{\upsilon}\right)\right]+\left(\int_0^t e^{-\beta(t-\tau)}Y_\rho(\upsilon\tau-2d)\,\mathrm{Sin}\,\bar{\omega}_{y\rho}(t-\tau)\,d\tau\right)\cdot H\left(1-\frac{2d}{\upsilon}\right)\right\} \quad (27a)$$

with $Q_y = \frac{M\upsilon^2}{4\cdot(R+e_H-b)}+\frac{M\upsilon^2}{4\cdot(R+e_H+b)}$ (27b)

where H is the Heaviside's unit function.

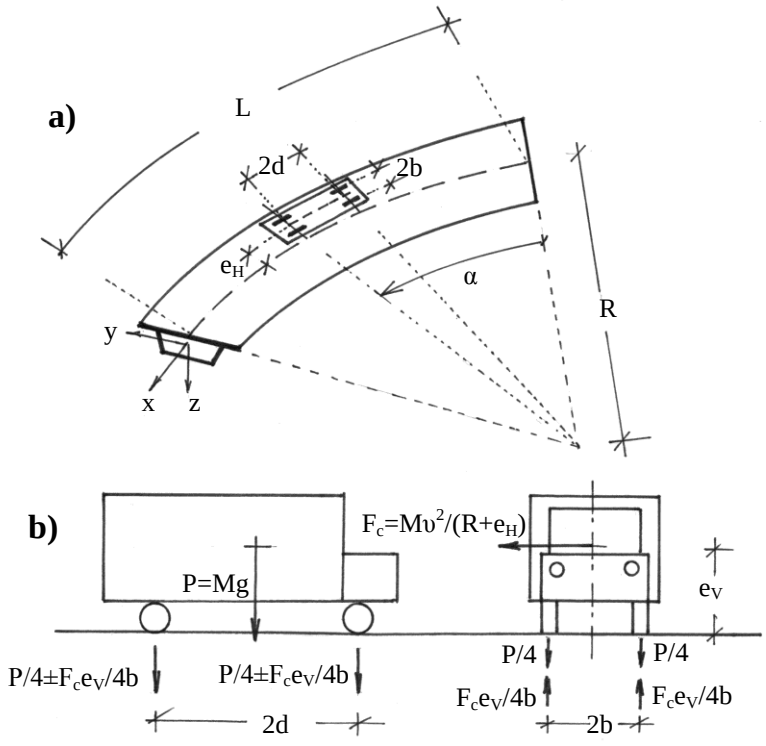

Fig. 4: The moving vehicle

5.2.2. The vertical-torsional motion

Introducing (26b,c) into the right side members of eqns (17a,b) and following the process of §4.2, we conclude to the following equation:

$$P_\rho(t)=\frac{1}{K_\rho}(R_{1\rho}(t)+Q_{1\rho}(t)+Q_{3\rho}(t))+\frac{1}{K_\rho}(R_{2\rho}(t)+Q_{2\rho}(t)+Q_{4\rho}(t)) \quad (28a)$$

where:

$$
\left.
\begin{aligned}
K_\rho &= \overline{\omega}_{z\rho}\left(m\int_0^L Z_\rho^2 dx + J_{px}\int_0^L \Theta_\rho^2 dx \right) \\
R_{1\rho}(t) &= \frac{Mg}{2}\left(\int_0^L e^{-\beta(t-\tau)} Z_\rho(\upsilon\tau)\,\mathrm{Sin}\,\overline{\omega}_{z\rho}(t-\tau)\,d\tau \right)\left(1 - H\left(t - \frac{L}{\upsilon}\right)\right) \\
R_{2\rho}(t) &= R_{1\rho}\left(t - \frac{2d}{\upsilon}\right) H\left(t - \frac{2d}{\upsilon}\right) \\
Q_{1\rho}(t) &= \left(\frac{Mg}{4} + \frac{F_c e_V}{4b}\right)(e_H + b)\cdot\left(\int_0^L e^{-\beta(t-\tau)} \Phi_\rho(\upsilon\tau)\,\mathrm{Sin}\,\overline{\omega}_{z\rho}(t-\tau)\,d\tau \right)\left(1 - H\left(t - \frac{L}{\upsilon}\right)\right) \\
Q_{2\rho}(t) &= Q_{1\rho}\left(t - \frac{2d}{\upsilon}\right) H\left(t - \frac{2d}{\upsilon}\right) \\
Q_{3\rho}(t) &= \left(\frac{Mg}{4} - \frac{F_c e_V}{4b}\right)(e_H - b)\cdot\left(\int_0^L e^{-\beta(t-\tau)} \Phi_\rho(\upsilon\tau)\,\mathrm{Sin}\,\overline{\omega}_{z\rho}(t-\tau)\,d\tau \right)\left(1 - H\left(t - \frac{L}{\upsilon}\right)\right) \\
Q_{4\rho}(t) &= Q_{3\rho}\left(t - \frac{2d}{\upsilon}\right) H\left(t - \frac{2d}{\upsilon}\right)
\end{aligned}
\right\} \qquad (28b)
$$

where H is the Heaviside's unit function.

6. NUMERICAL RESULTS AND DISCUSSION

Let us consider a curved-in-plane bridge, with length L=60 m (see fig. 4). The bridge is made from structural steel (isotropic and homogeneous material) with modulus of elasticity E=2,1x10^{8}kN/m^2, shear modulus G=0,8x10^{8}kN/m^2, moments of inertia J_y=0.50m^4, J_z=8,00m^4, torsional constant J_d=0,50m^4, warping constant J_ω=0,25m^6, mass per unit length m=1200 kg/m and mass moment of inertia J_{px} =10200 kgm^2. Three characteristic radius of curvature are studied: R=50m, R=100m, and R=150m.

We will study the dynamic behavior of the bridge under the action of:

a. A concentrated moving load with speed υ and magnitude $P = M \cdot g$ and M=40 000kg.
b. A sequence of two concentrated loads spaced 2d with magnitude $P_1 = P_2 = M \cdot g/2$.
c. A real vehicle of dimensions 2d*2b, whose the tires are considered as concentrated loads.

According to the results of table 1, the studied speeds must be less than $\upsilon = 35\ \mathrm{m/sec}$.

6.1. The concentrated moving load

6.1.1. The lateral motion

- The radius of curvature

The plots of figure 5 show the lateral vibrations of the mid-span of the bridge (x=L/2) for
speeds υ =10 m/sec (fig 5a), υ =20 m/sec (fig 5b), and υ =30 m/sec (fig 5c) and various radii of curvature R.

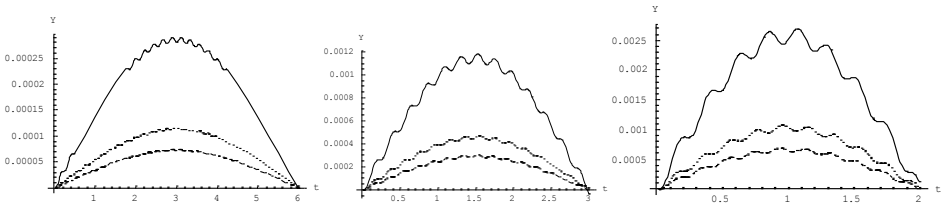

(a) υ =10 m/sec (b) υ =20 m/sec (c) υ =30 m/sec

Figure 5: The influence of the radius of curvature for
___ R=50 m, …… R=100 m, - - - R=150 m

As it was expected, we observe that for small R the developed deflections are much greater than the ones for great R. These differences amount:
Between R=100 and R= 150 the difference amounts to about 150%
Between R=50 and R= 100 the difference amounts to about 250%
Between R=50 and R= 150 the difference amounts to about 400%
These percentage differences are slightly affected by the value of speed υ.

- The eccentricity

The plots of figure 6 show the lateral vibrations of the mid-span of the bridge (x=L/2) for υ =30 m/sec, radii of curvature R=50m(fig 6a), R=100m (fig 6b) and R=150m (fig 6c), for various eccentricities e_H.

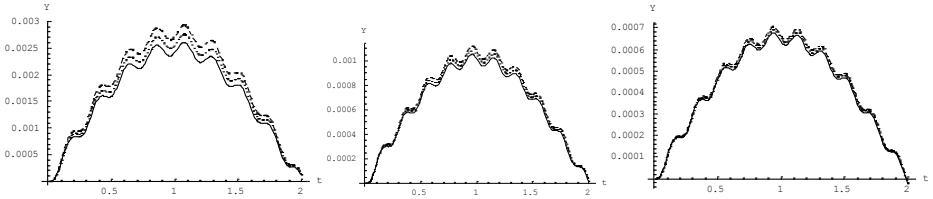

(a) R=50m (b) R=100 m (c) R=150 m

Figure 6: The influence of the eccentricity for υ = 30 m/sec and
___ e_H=3 m, …… e_H=0 m, - - - e_H= -3 m

From these plots we see that as the R increases the influence of the eccentricity e_H on the bridges' deflections decreases. For R=50 and υ = 30 the difference between e_H=3 and e_h=-3 amount to about 15%, while for R=150 and υ = 30 the difference between e_H=3 and e_h=-3 amount to about 3%

- The speed

Finally in figure 7 we see the deflections of the mid-span of the bridge for R=50, e_H=0 and various values of speed.

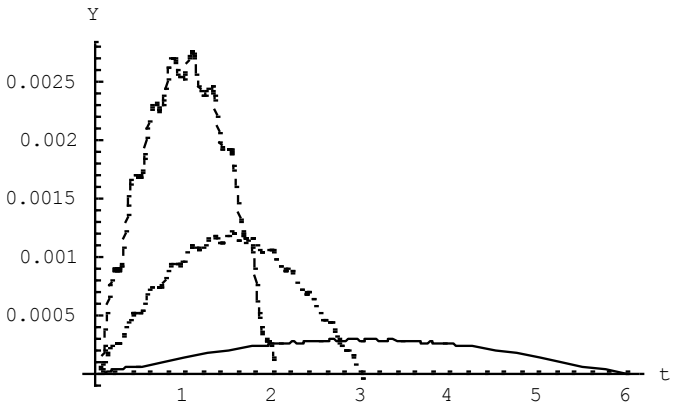

Figure 7: The influence of the speed for R=50 m, e_H=0 m and
υ =10m/sec (___), υ =20m/sec (……), υ =30m/sec (- - -)

6.1.2. The vertical-torsional motion

- The speed

The plots of figure 8 show the vertical-torsional vibrations of the middle of the bridge (x=L/2) for R=50m, eccentricity e_H=3 m, and e_V=1.20 m.

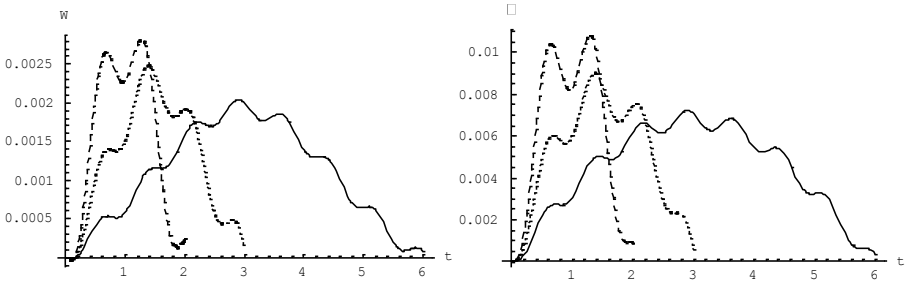

Figure 8: The influence of the speed for R=50m, e_H=3 m, e_V=1.20 m, and
υ =10m/sec (___), υ =20m/sec (……), υ =30m/sec (- - -)

The plots of figure 9 show the vertical-torsional vibrations of the mid-span of the bridge (x=L/2) for R=100m, eccentricity e_H=3 m, and e_V=1.20 m.

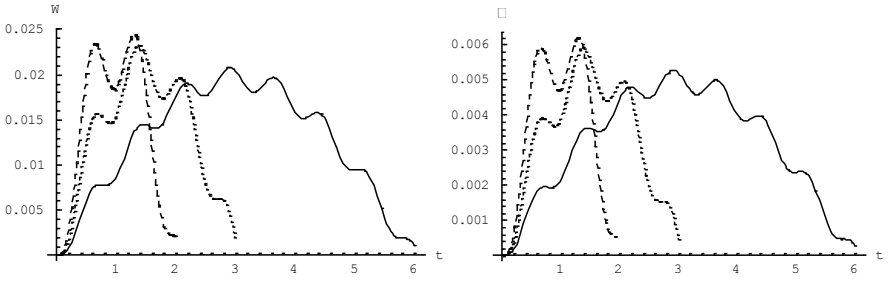

Figure 9: The influence of the speed for R=100m, e_H=3 m, e_V=1.20 m, and
υ =10m/sec (___), υ =20m/sec (……), υ =30m/sec (- - -)

The plots of figure 10 show the vertical-torsional vibrations of the mid-span of the bridge (x=L/2) for R=150m, eccentricity e_H=3 m, and e_V=1.20 m.

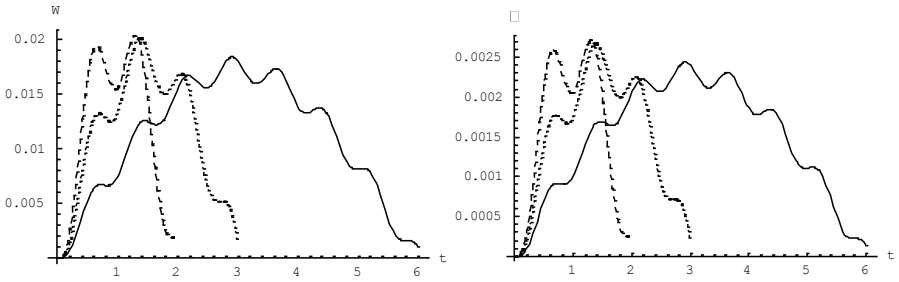

Figure 10: The influence of the speed for R=150m, e_H=3 m, e_V=1.20 m, and
υ =10m/sec (___), υ =20m/sec (……), υ =30m/sec (- - -)

From the above plots we ascertain that for both deformations (deflection and rotation angle), the influence of the speed is greater in bridges with small radius of curvature than in bridges with great ones. For the cases studied this influence amounts to about 60 – 70% for R=50 m decreasing to about 10 – 20% for R=150 m.

- The radius of curvature

The plots of figure 11 show the vertical-torsional motion of the middle of the bridge (x=L/2) for speed υ =20 m/sec, e_H=1.50 m, e_V=1.20 m, and various radii of curvature.

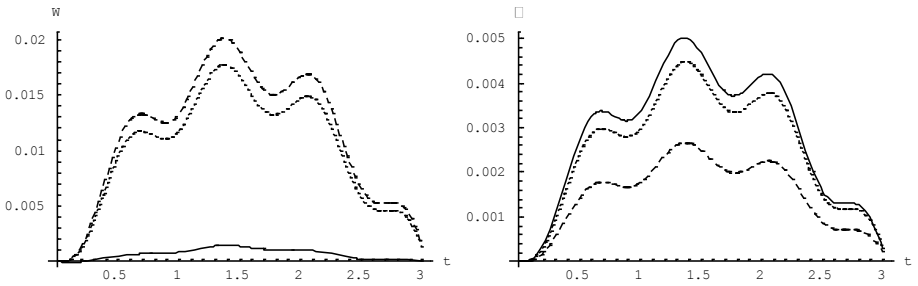

Figure 11: The influence of radius of curvature for υ = 20 m/sec, e_H=1.5m, e_V=1.2m and R=50m (___), R=100m (…..), R=150m (- - -)

- The eccentricity

The plots of figure 12 show the vertical-torsional vibrations of the mid-span of the bridge (x=L/2) for R=50m, υ = 30 m/sec, and various values of eccentricity.

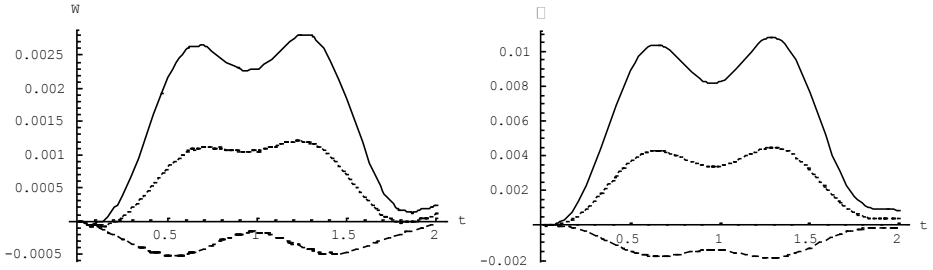

Figure 12: The influence of eccentricity for υ = 30 m/sec, R=50 m, and ___ e_H=3 m, …… e_H=0 m, - - - e_H= -3 m

The plots of figure 13 show the vertical-torsional vibrations of the mid-span of the bridge (x=L/2) for R=100m, υ = 30 m/sec, and various values of eccentricity.

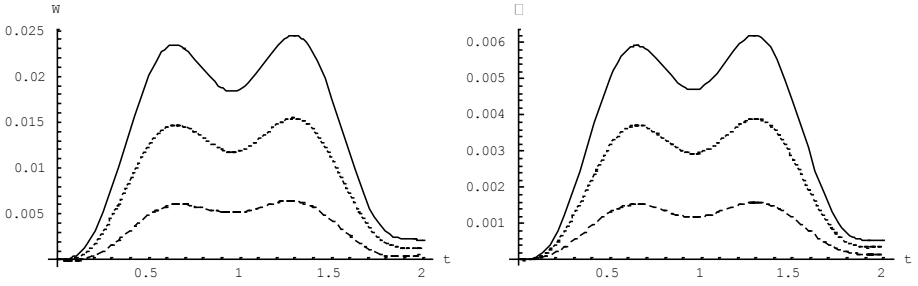

Figure 13: The influence of eccentricity for υ = 30 m/sec, R=100 m, and ___ e_H=3 m, …… e_H=0 m, - - - e_H= -3 m

The plots of figure 14 show the vertical-torsional vibrations of the mid-span of the bridge (x=L/2) for R=150m, υ = 30 m/sec, and various values of eccentricity.

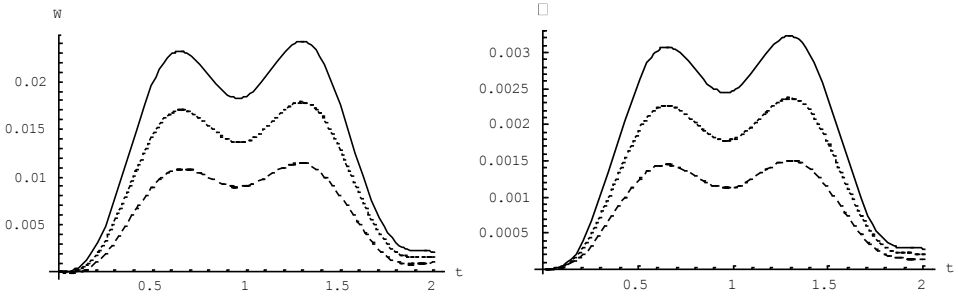

Figure 14: The influence of eccentricity for υ = 30 m/sec, R=150 m, and
___ e_H=3 m, …… e_H=0 m, - - - e_H= -3 m

From the plots of figure 12 we observe that for eccentricity e_H=-3m, both deformations (deflection and rotation angle) are negative. This, was expected for the rotation angle, but not for the deflection. However this deflection is referred to the axis of the cross-section, while the deflection of the point where the load is applied is:

$$-0.0005+(-3)\cdot(-0.002)=+0.0055>>\left|-0.0005\right|.$$

6.2. The moving vehicle

6.2.1. The lateral motion

- The model influence

The plots of figure 15 show the lateral motion of the mid-span of the bridge (x=L/2), for υ = 30 m/sec, e_H=3.00m, e_V=1.20m and various values of curvature.

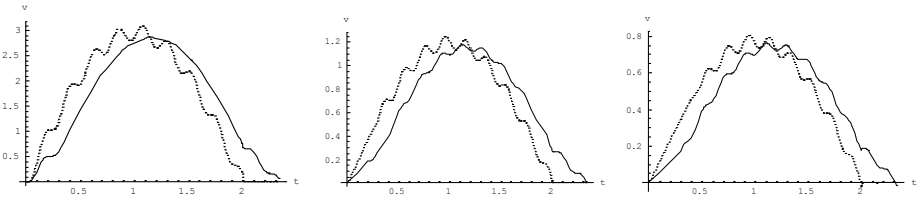

(a) R=50 m (b) R=100 m (c) R=150 m

Figure 15: The influence of the used model for υ = 30 m/sec, e_H=3.00m, e_V=1.20m, for a vehicle with wheelbase 2d=10m (___), one concentrated load (- - -)

From the above plots we see that the radius of curvature has little effect on the lateral vibrations of the bridge. This effect ranges from 6 to 10%.

- The influence of wheelbase 2d

The plots of figure 16 show the lateral motion of the mid-span of the bridge (x=L/2), for R=50m, υ = 30 m/sec, e_H=3.00m, e_V=1.20m and various values of the vehicle's wheelbase 2d.

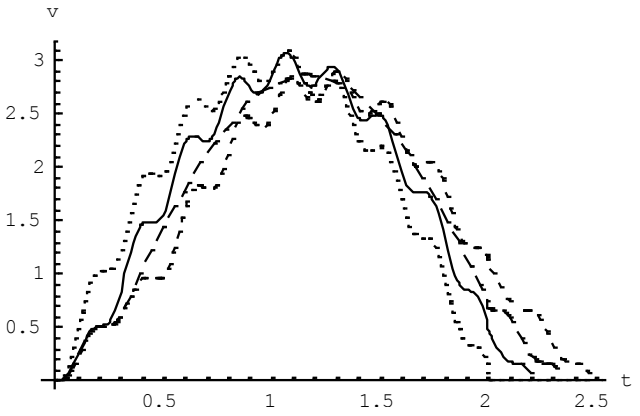

Figure 16: The influence of the vehicle's wheelbase for R=50m, υ = 30 m/sec, e_H=3.00m, e_V=1.20m and d=3m (__), d=5m (_ _), d=7m (- - -) and d=0m (….)

The plots of figure 17 show the lateral motion of the mid-span of the bridge (x=L/2), for R=100m, υ =30 m/sec, e_H=3.00m, e_V=1.20m and various values of vehicle's wheelbase 2d.

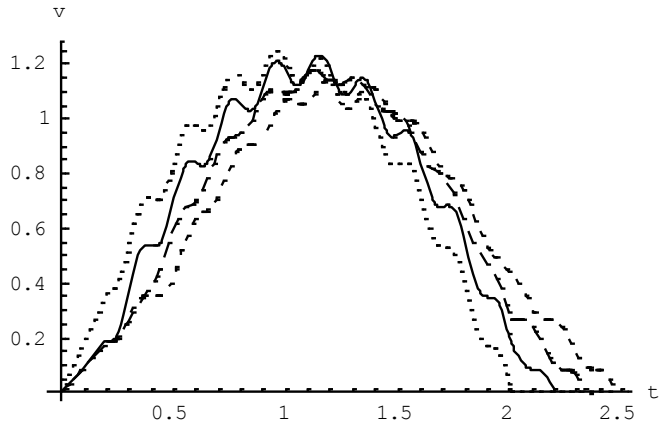

Figure 17: The influence of the vehicle's wheelbase for R=100m, υ = 30 m/sec, e_H=3.00m, e_V=1.20m and d=3m (__), d=5m (_ _), d=7m (- - -) and d=0m (….)

The plots of figure 18 show the lateral motion of the mid-span of the bridge (x=L/2), for R=150m, υ = 30 m/sec, e_H=3.00m, e_V=1.20m and various values of vehicle's wheelbase 2d.

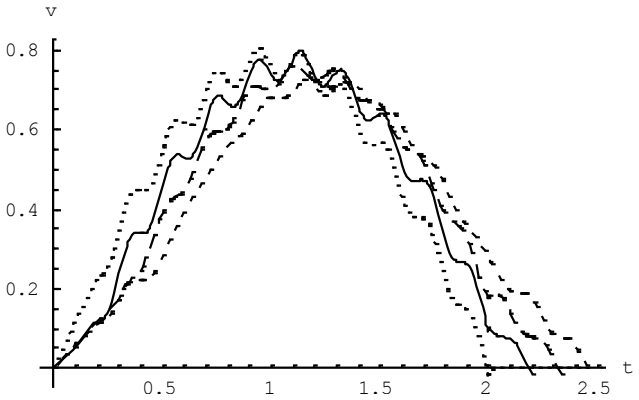

Figure 18: The influence of the vehicle's wheelbase for R=150m, υ = 30 m/sec, e_H=3.00m, e_V=1.20m and d=3m (__), d=5m (_ _), d=7m (- - -) and d=0m (….)

From the above plots we see that the vehicle's wheelbase has small influence on the lateral vibrations of the bridge. This effect ranges from 4 to 8%.

6.2.2. The vertical-torsional motion

- The model influence

The plots of figure 19 show the vertical-torsional motion of the mid-span of the bridge (x=L/2), for R=50m, υ = 30 m/sec, e_H=3.00m, e_V=1.20m for the three models of loading, one model of a real vehicle of dimensions 2d * 2b, one model consisted by a sequence of two concentrated loads and one model consisted by one concentrated load. We observe that for this value of R the differences are great.

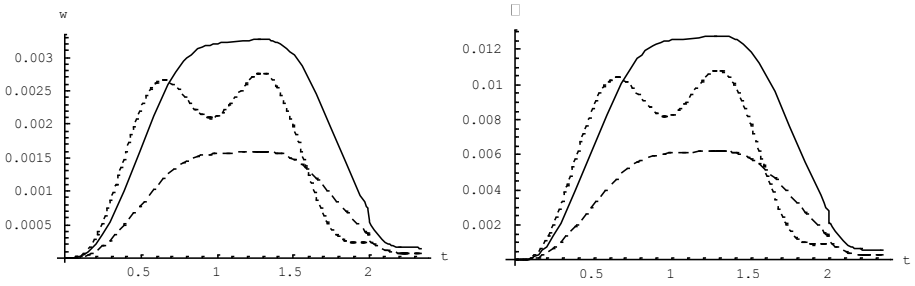

Figure 19: The vertical-torsional motion of the mid-span of the bridge (x=L/2), for R=50m, υ = 30 m/sec, e_H=3.00m, e_V=1.20m, d=5m for the three models of loading (__) the real vehicle, (- - -) sequence of two loads, (….) one concentrated load

The plots of figure 20 show the vertical-torsional motion of the mid-span of the bridge (x=L/2), for R=100m, υ = 30 m/sec, e_H=3.00m, e_V=1.20m, for the three models of loading, one model of a real vehicle of dimensions 2d * 2b, one model consisted by a sequence of two concentrated loads and one model consisted by one concentrated load.

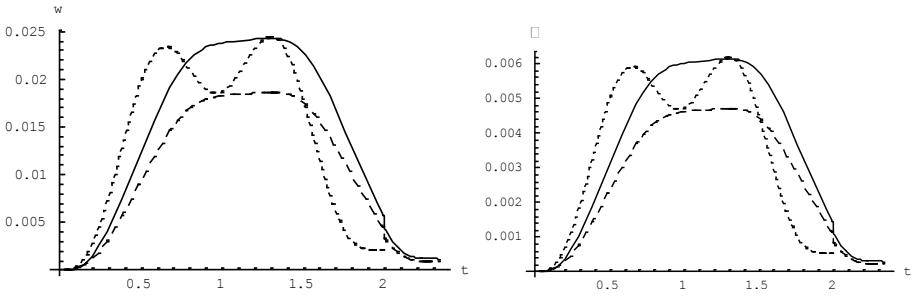

Figure 20: The vertical-torsional motion of the mid-span of the bridge (x=L/2), for R=100m, υ = 30 m/sec, e_H=3.00m, e_V=1.20m, d=5m for the three models of loading (__) the real vehicle, (- - -) sequence of two loads, (….) one concentrated load

The plots of figure 21 show the vertical-torsional motion of the mid-span of the bridge (x=L/2), for R=100m, υ = 30 m/sec, e_H=3.00m, e_V=1.20m for the three models of loading, one model of a real vehicle of dimensions 2d * 2b, one model consisted by a sequence of two concentrated loads and one model consisted by one concentrated load.

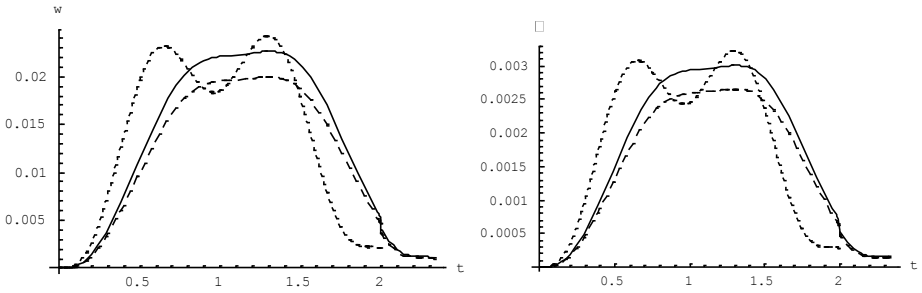

Figure 21: The vertical-torsional motion of the mid-span of the bridge (x=L/2), for R=150m, υ = 30 m/sec, e_H=3.00m, e_V=1.20m, d=5m for the three models of loading (__) the real vehicle, (- - -) sequence of two loads, (….) one concentrated load

From figure 19, we see that for small radii of curvature the choice of the right model affects the results too much. We see also that the model of a sequence of

two concentrated loads leads to inaccurate results. This error amounted to about 100%.
From the plots of figures 20 and 21 we see that always the above model of a sequence of two loads is most inaccurate with errors amounted from 15 to 25%.

- The influence of wheelbase 2d

The plots of figure 22 show the lateral motion of the mid-span of the bridge (x=L/2), for R=50m, υ = 30 m/sec, e_H=3.00m, e_V=1.20m and various values of vehicle's wheelbase 2d.

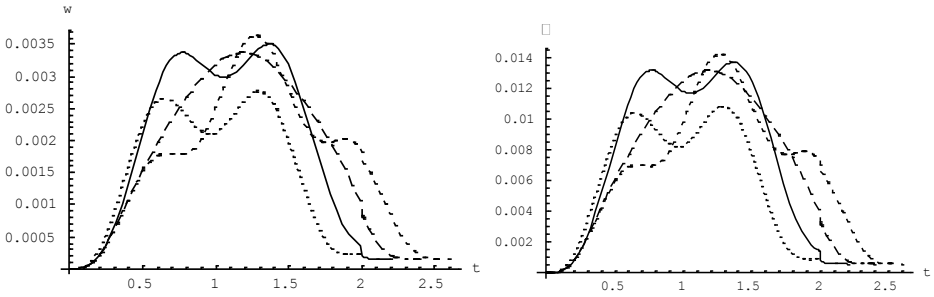

Figure 22: The influence of the vehicle's wheelbase for R=50m, υ = 30 m/sec, e_H=3.00m, e_V=1.20m and d=3m (__), d=5m (_ _), d=7m (- - -) and d=0m (….)

The plots of figure 23 show the lateral motion of the mid-span of the bridge (x=L/2), for R=100m, υ = 30 m/sec, e_H=3.00m, e_V=1.20m and various values of vehicle's wheelbase 2d.

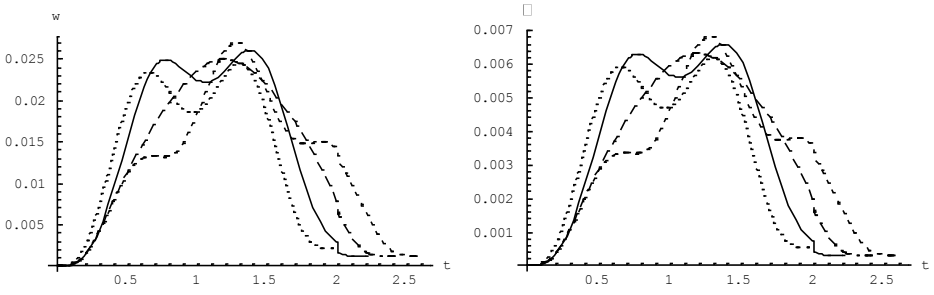

Figure 23: The influence of the vehicle's wheelbase for R=100m, υ = 30 m/sec, e_H=3.00m, e_V=1.20m and d=3m (__), d=5m (_ _), d=7m (- - -) and d=0m (….)

The plots of figure 24 show the lateral motion of the mid-span of the bridge (x=L/2), for R=150m, υ = 30 m/sec, e_H=3.00m, e_V=1.20m and various values of vehicle's wheelbase 2d.

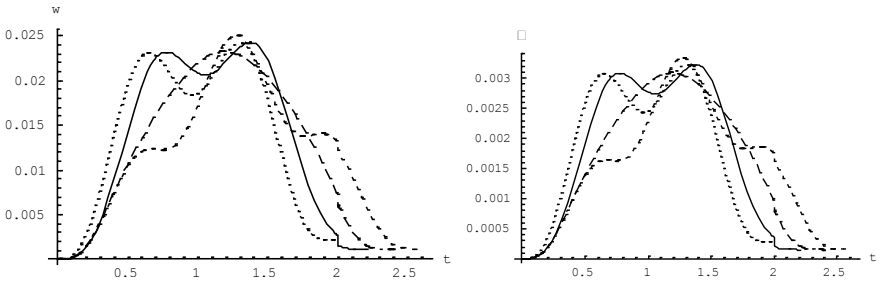

Figure 24: The influence of the vehicle's wheelbase for R=150m, υ = 30 m/sec, e_H=3.00m, e_V=1.20m and d=3m (__), d=5m (_ _), d=7m (- - -) and d=0m (….)

From the above plots we see that for small radii of curvature (R=50m), the model of one concentrated load is the most inaccurate (error ~20%). The other three models give somewhat similar results.
For greater radii of curvature (R=100 or 150m), all models give similar results as regarding the maximum deformations. Existing differences amount to about 3 to 6%. Note that each model gives a different view of the bridge deformations. For example the models with d=3 and d=5m give one maximum while the ones with d=0 and d=7m give two maxima.

7. CONCLUSIONS

From the chosen data of bridges' characteristics and of moving loads' models, one can draw the following conclusions:

1. A mathematical model for the study of curved-in-plane bridges is presented.
2. As for the surface conditions of the deck, we see that for wet surfaces the value of a safe speed decreases dramatically (24 to 27% for R=50 to 150 m). The use of section slope (super-elevation) improves significantly the value of the allowed safe speed (~16%).
3. The radius of curvature strongly affects the lateral motion.
4. For the vertical-torsional motion and for small values of radius of curvature, sometimes, negative deflections of the bridge's axis are computed, while the deflections of the points where the load applies have positive values much higher than the ones of the bridge's axis.
5. The above mentioned deformations are affected by the eccentricity of the applied load. This influence amounts from 3 to 15%.
6. In bridges with small radii of curvature, models corresponding to actual real models of loading should be employed. In this case it is recommended to avoid the use of one concentrated load model, because the calculated error is high.

7. Finally, as for the distance of vehicles' axles, the use of the real data is critical not only to determine the exact value of the maximum deflections but also to achieve the right view of the bridges' deflections.
8. For L/2d >~ 7, the resulting maximum values of deformations are not severely affected by the use of any loading model.

REFERENCES

1. Frýba, L.,1972, *Vibrations of solids and structures under moving loads*. Groningen, Nordhoff International Publication Co,.
2. Stokes, 1849, "G.G., Discussion of a differential equation relating to the breaking of railway bridges", *Transactions of the Cambridge Pholosophical Society*, 707-735.
3. Zimmermann, H., 1896, "Die Schwingungen eines Trägers mit bewegter Last', *Centralblatt der Bauverwaltung*, [16, (23), 249-251], [23A, 257-260], [24, 264-266], [26, 288].
4. Krýlov, A.N., 1905, "Über die erzwungenen Schwingungen von gleichförmigen elastigchen Stäben". *Mathematical Annalen*, 61, 211.
5. Timoshenko, S.P., 1922, "On the forced vibration of bridges". *Philosophical Magazine*, Series 6, 43 1018.
6. Inglis C.E. , 1934, *"A Mathematical Treatise on Vibration in Railway Bridges",* The University Press, Cambridge.
7. Hillerborg, A., 1951, "*Dynamic influences of smoothly running loads of simply supported girders"*, Kungl. Tekhn. Högs kolan, Stockholm.
8. Steuding, H., "Die Schwingungen von Trägern bei bewegten Lasten I, II". *Ingenieur Archiv*, 1934, 5(4), 275-305 / 1935, 6(4), 265-270.
9. Honda, H., Kajikawa, Y. and Kobori, T., 1982, "Spectra of road surface roughness on bridges", *Journal of Structure Engineering ASCE*, 108(9).
10. Gillespi, T.D. and al, 1993 "*Effect of heavy vehicle characteristics on pavement response and performance"*, NCHRP, Rep. 353, Trans Res. Board (TRB), Washington D.C.,.
11. Green, M.F., Cebon, D., Cole,D.J., 1995, "Effects of Vehicle Suspension Design on Dynamics of highway Bridges". *Journal of Structural Engineering*, 121(2).
12. Lee, H.P., 1996, "Dynamic response of a Beam with a moving mass". *Journal of Sound and Vibrations*, 191(2)
13. Michaltsos, G.T., Sophianopoulos, D. and Kounadis, A.N., 1996, "The effect of a moving mass and other parameters on the dynamic response of a simply supported beam". *Journal of Sound and Vibration*, 191(3), 357-362.
14. Xu, X., Xu, W., Genin, J., 1997, "A non linear moving mass problem". *Journal of Sound and Vibrations*, 204(3)
15. Foda, M.A., Abduljabbar, Z., 1972, "A Dynamic Green Function Formulation for the response of a Beam structure to a moving Mass", *Journal of Sound and Vibration*, 1998, 210(3).
16. Michaltsos G.T. 2001, "The influence of Centripetal and Coriolis forces on the dynamic response of light bridges under moving vehicles". *Journal of Sound and Vibration*, 247(2), 261-277
17. Michaltsos G.T. 2002, "Dynamic behaviour of a single-span beam subjected to load moving with variable speeds". *Journal of Sound and Vibration*, 258(2), 359-372.
18. Am. Association of State, 12th edition, Hwy and transp. Officials (AASHTO), Washington D.C., 1977."*Standard specifications for highway bridges".*
19. Ministry of Transpor. And Communications, Downsview, Ontario, Canada, 1983. *Ontario highway bridge design code*, Ontario
20. Council of Eur. Communities, 1992, Council Directive, 92/7/EEC amending Directive *85/3/EEC on the weights, dimensions and certain technical characteristics of certain road vehicles* , Brussels, Belgium..

21. ISO/TC 108/WG9 Draft No 3c, Int. Organization for Standarization (ISO), Geneva, Switzerland, 1972. "*Proposals for generalized road inputs to vehicles".*
22. Cantieri, R., , 1991, "*Beitrag zur dynamik von Strassenbrucken unter der uberfahrt schwerer Fahrzeuge",* Diss. ETH Nr 9505, Technische hochschule, Zurich.
23. Mozer J, Culver C, 1970, "Horizontally curved highway bridgesStability of curved plate girders". *Report no.P1, research project HPR-2(111*), Carnegie Mellon University, Pittsburgh
24. Culver C, 1972, "Design recommendations for curved highway bridges". *Final report for research project 68-32*. Pennsylvania Department of Transportation, Harrisburg
25. Brennan PJ, 1974, "Analysis and structural testing of a multiple configuration small scale horizontally curved highway bridge". *Research project HPR-2(111),* Syracuse University, Syracuse
26. Yoo CH, Carbine RL (1985) Experimental investigation of horizontally curved steel wide flange beams analysis. In: Proceedings structural stability research council annual technical session: stability aspects of industrial buildings, pp 183–191
27. Zureick A, Naqib R, Yadlosky JM, 1994, "Curved steel bridge research project, interim report I: synthesis". HDR Engineering, Pittsburgh. Publication Number FHWA-RD-93-129
28. CEN, 2006, Eurocode 8. Design of structures for earthquake resistance: Part 2. Bridges. CEN, Brussels
29. Caltrans, 2006, "Seismic design criteria 1.4. California Department of transportation, Sacramento, CA.
30. Abdel-Salam MN, Heins CP, 1988, "Seismic response of curved steel box girder bridges". *J Struct Eng* 114(12):2790–2800
31. Wu H, Najjar WS, 2007, "Parametric seismic analysis of curved steel box-girder bridges with two continuous spans", *Bridge Struct* 3(3, 4):205–213
32. Linzell DG, Nadakuditi VP, 2011, "Parameters influencing seismic response of horizontally curved, steel, I-girder bridges", *Steel Compos Struct* 11(1):21–38
33. Raftoyiannis I, Michaltsos G.T., 2012, "Curved in plane Cable-Stayed-Bridges. A mathematical model", *Int. Journal of Struct. Stability and Dynamics,*12(3).

Received: Dec 15, 2014 Accepted: May 6, 2015